Skid Resistance: Understanding the Role of Road Texture Scales using a Signal Decomposition Technique and a Friction Model

1. ABSTRACT

Skid resistance markedly depends upon road surface characteristics, particularly to its texture. Texture can be considered to be composed of a range of different scales each of which contributes differently to the generation of adequate friction at the tire-road interface in wet conditions. This work aims to contribute to understanding the role of these different scales.

The method adopted deploys a signal processing technique, termed Empirical Mode Decomposition, to decompose the road surface texture into a set of component profiles of different wavelengths. The Dynamic Friction Model, a computational friction model already validated on real road surfaces, is then used to determine the relative effect of partially recomposed profiles with their components on skid resistance.

The results demonstrate the importance of not only "small-scale" and "large-scale" textures but also their spatial arrangement and shape. Indeed, on wet road surfaces, "small-scale-texture" was found to be key to achieving good skid resistance at low speeds, whilst "large-scale-texture" was found to be crucial to maintaining it with increasing speed.

But furthermore, the distribution of the summits of the large-scale-textures was established as being able to compensate for a lack of small-scale-texture. Conversely, the reverse was established as also being true, with the small sharp local summits of small-scale-texture being found to compensate for a lack of large-scale-texture. Even though it should be noted that this random distribution and the pointed shape of the summits may also be an inconvenience with respect to other surface properties such as noise and rolling resistance.

2. KEYWORDS

Texture, Small-scale-texture, Large-scale-texture, Skid resistance, Dynamic Friction Model, Empirical Mode Decomposition

3. INTRODUCTION

Adequate skid resistance [1] is key to vehicles' safe transit upon roads. It describes the contribution that the road makes to tire/road friction. The textures of these road surfaces and in particular the scales termed "Macrotexture" and "Microtexture" [ISO 13473-2] remain the principal parameters governing that skid resistance. Macrotexture refers to the texture of wavelengths of between 0.5 and 50 mm and amplitudes of between 0.2 and 10 mm. The Macrotexture is mainly dictated by among others the shape, size, and gradation of the aggregates in the pavements and is widely accepted as making the main contribution to water drainage out of the tire-road contact patch. Microtexture refers to the texture of smaller wavelengths of between 0 and 0.5 mm and of amplitudes of between 0 and 0.2 mm. Microtexture is mainly dictated by among others the micro-asperities upon the surface of the aggregates and is known to break any residual water film in tire-road contact patch to restore partially a direct contact between the two tire and road surfaces.

Within this paper, instead of precisely defining texture scales as 'Microtexture' and 'Macrotexture', 'Small-Scale-Texture'(SST) and 'Large-Scale-Texture' (LST) will be adopted, this dictated by texture decomposition method adopted in this work that decomposes the road surface texture to naturally inherent and not pre-defined different scales. LST is defined as the texture wavelengths and amplitudes equivalent to the size of road surface aggregates. Similarly, SST is defined as the texture wavelengths and amplitudes equivalent to the size of the roughness present upon the surface of these aggregates. Instead of the common 0.5 mm corresponding to the lower microtexture wavelengths, the lower limit of the SST is set to 0.87 mm due to the resolution of the used profilometer to capture the topography of the surface in this work that is equal to 0.87 mm (See section 6 and the reference : [ASTM E1960 2011, 2015]. However, to not forget the contribution of the wavelengths from 0.5 to 0.87 mm, a local friction coefficient is introduced in the calculations (see equation 2 and the reference: [Kane et al., 2015, 2017]).

In view of the importance of these two texture scales for skid resistance in wet conditions as specified above, their presence on road surfaces is ensured by specifying the components and the design of the pavement before construction. SST is provided by aggregates selected on the capacity to stay unpolished when subjected to the traffic. The mineralogical composition, of

[1] **Skid resistance** is a measurement of friction obtained under specified, standardized conditions, generally chosen to fix the values of many of the potential variable factors so that the contribution that the road provides to tire/road friction can be isolated [Kane, Scharnigg, 2009].

aggregates comprised primarily of hard quartz mineral particles cemented together with a softer mineral matrix, like Greywacke aggregate, maintain long term adequate SST as a consequence of the differential wear and debonding of individual particles under traffic [Masad et al., 2009; Kane et al., 2013]. LST depends upon the shape, size, and gradation of the coarse aggregates, with coarse aggregates dominating LST when they are closely packed [Hall et al. 2009].

To determine the role of these texture scales, many investigations have been already undertaken. Sabey's experimental tests showed in the 1950s that in wet conditions at low speeds, that higher LST and SST benefit skid resistance [Sabey 1958]. At higher speeds, lowering LST leads to a reduction in available skid resistance. The effect of these both texture scales on speed-dependent wet skid resistance has been repeatedly confirmed and empirically modeled [Leu et al., 1983; Fwa, 2017]. As an example, one can consider the International Friction Index (IFI) and the Penn State model derived from statistical fittings of measured skid resistance data [ASTM 1998 E1960-98; Kulakowski, 1991]. These models represent the graphical curve of skid resistance versus speed by means of equations with two parameters. The first parameter, the intercept, occurring at zero vehicle speed is related to SST, whilst the second parameter describes the shape of the curve and is related to the LST. However, even if these studies allowed a better understanding of the role of the texture scales, they completely ignored the effect of their spatial distribution.

To go further in the understanding of the texture scales' effects, mathematical methods of signal decomposition like Fractals, Fourier, Wavelet Transforms have been explored, considering the decomposition of road surface texture. Attempts, to couple contact models to surface textures approximated from their fractal's parameters, have been undertaken to correlate skid resistance to texture [Rado 1996, Gert 1997, Villani et al. 2011]. Villani et al. calculated the hysteresis contribution to friction by means of an analytical model of a sliding elastomer passing over a road surface with a texture described from its fractal dimension. But, despite the significant advances in friction modeling, no conclusion has been drawn about the role of the different texture scales and their spatial distribution.

Recently, Kane et al. found a statistical correlation to skid resistance [Kane et al., 2014] after calculating a set of texture parameters from amplitudes and frequencies using functions derived from an Empirical Mode Decomposition (EMD) [Huang et al., 2006; Cho, 2010]. Furthermore, Kane et al. developed and validated a computational model the 'Dynamic Friction Model' (DFM) to predict the skid resistance of roads using their topographies [Kane et al., 2015, 2017]. Based on these two above studies by synergizing the EMD and DFM, the present work tries to

contribute to the effort of identifying the role of SST and LST on skid resistance in wet conditions. The method adopted will be based on the different steps:

- The extraction of the inherent road surface basic profiles of different wavelengths from the original road surface profile using the EMD,
- The recombination of new profiles using these basic profiles to produce a set of new profiles of different levels of SST and LST,
- And the use of the DFM on these new profiles to determine the relative effect of SST and LST.

4. REVISITING THE DFM

The basic equations of the DFM derive from balancing the forces acting at the contact point between the road and a moving rubber element (equation 1 & Figure 1) [Kane et al., 2017].

$$\overrightarrow{F_{ij}} + \overrightarrow{T_{ij}} + \overrightarrow{R_{ij}} + \overrightarrow{FR_{ij}} = \vec{0} \qquad \text{Equation 1}$$

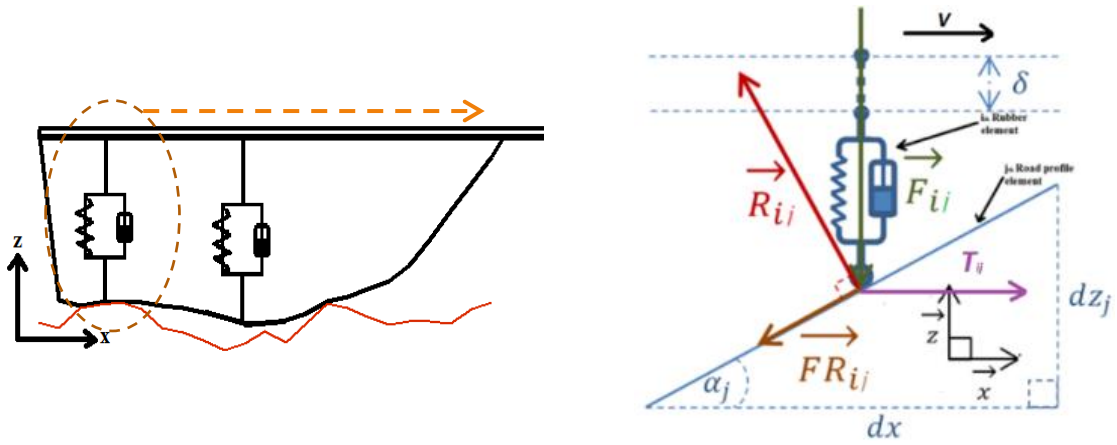

Figure 1: Forces acting in the contact point between a rubber element and a road profile

Where, $\overrightarrow{F_{ij}}$ is the force applied by the rubber element on the road surface. The force, it is calculated using a "Kelvin-Voigt" model, where K is the spring's elastic modulus and C is the dashpot's viscosity. $\overrightarrow{F_{ij}}$ is balanced by the load through the integrated respective components of the contact pressure p_{ij}.

$$F_{ij}(t) = l \times dx \times p_{ij}(t) \text{ with } p_{ij}(t) = Ku_{ij}(t) + C\frac{du_{ij}(t)}{dt} \text{ and } u_{ij}(t) = \delta(t) - h_i + z_j$$

With, t representing the time and $u_{ij}(t)$ the displacement of the rubber i^{th} element contacting j^{th} element on the road at time t. $\delta(t)$ is the solid displacement of the pad at t. h_i represents the pad

geometry. z_j is the height of the j^{th} point of the road profile. $\overrightarrow{T_{lj}}$ is the traction force. $\overrightarrow{R_{lj}}$ is the surface reaction force. $\overrightarrow{FR_{lj}}$ is a local friction force. $FR_{ij} = \mu_{\mathbf{loc}} R_{ij}$ when the element is moving on a "pseudo smooth inclined plane" with angle α_j and where $\mu_{\mathbf{loc}}$ represents a local friction coefficient. The projection of equation 1 in local contact coordinates, onto global contact coordinate's axes x and z, coupled with the condition that $FR_{ij} = \mu_{loc} R_{ij}$ leads to:

$$T_{ij}(t) = F_{ij}(t)\frac{\sin(\alpha_j) + \mu_{loc}\cos(\alpha_j)}{\cos(\alpha_j) - \mu_{loc}\sin(\alpha_j)} \qquad \text{Equation 2}$$

When an element is not in contact with the road surface, its contact pressure is nil and the rubber element is subjected to a relaxation phase. Its position on the Z-axis is then determined by solving equation 3:

$$Ku_{ij}(t) + C\frac{du_{ij}(t)}{dt} = 0 \qquad \text{Equation 3}$$

At any time the load *W* applied on the pad must be balanced by the sum of the normal contact pressures:

$$W = \sum_i^N F_{ij}(t) \qquad \text{Equation 4}$$

Where N is the number of discrete elements of the rubber pad. Accordingly, the global skid resistance $\mu_j(t)$ can then be calculated using the following formula:

$$\mu_j(t) = \frac{\sum_i^N T_{ij}(t)}{W} \qquad \text{Equation 5}$$

At this stage, the only unknown factors are those relating to $F_{ij}(t)$, representing the contact force applied by the rubber elements on the road surface. To obtain the calculation details of these dynamic viscoelastic contact forces, the reader is advised to refer to the following publication [Kane et al., 2015, 2017].

To take into account the water in the contact patch, a simplification is adopted. The contact geometry is approached as an equivalent hydrodynamic bearing. The equivalent geometry of that hydrodynamic bearing is estimated from the water thickness at the surface and the "opening spaces" available in the contact. At each calculation iteration, its load capacity is estimated and subtracted to the normal load. The reader is advised to refer to Kane's publication [Kane et al. 2017] to get the details.

$$W_h = \frac{\alpha 6\eta V^{\beta} l L^2}{H_{out}^2 (a-1)^2}\left[\log(a) - 2\frac{a-1}{a+1}\right] \qquad \text{Equation 6}$$

Where, $a = \frac{H_{in}}{H_{out}}$, with H_{out} and H_{in} are respectively the outlet and inlet water thicknesses of the simplified hydrodynamic bearing. η is the water viscosity. L and l are the lengths and the width of the bearing, in this case, the rubber pad. α et β are two empirical coefficients (10^5 and 1.75 respectively) added to adjust the load-bearing capacity of the hydrodynamic bearing component.

To learn more about the formalism details and the validation with field data of the DFM, the readers are advised to refer to the publications Kane et al. 2017 and 2018 on the references list.

5. SELECTING THE TESTED SURFACES

The specified test surfaces represent a range of different morphologies to cover a broad combination of both SST and LST (Figure 2). They are composed of an artificial surface and a set of selected surfaces located on the Ifsttar[2] test track, located near Nantes in France:

- The artificial surface is fabricated by sticking rounded and sandblasted aggregates onto a plate. This surface is considered as "Analytical Surface" because of the clear distinguishability of the LST and SST, corresponding respectively to the average size of the rounded aggregates and the impacts left by the sandblasting procedure.
- The other surfaces are selected from the Ifsttar test track to cover a broad combination of LST and SST. These "Test-Track Surfaces" feature some surfaces with "extreme" textural characteristics, i.e. a smooth resin finish, calcined bauxite, painted surfaces, etc. Other track test sections are representative of actual pavements laid on the national highways like Porous Asphalt, Very Thin Asphalt Concrete, etc.

Analytical Surface

Test track surfaces

Figure 2: Analytical Surface on the left and test track surfaces on the right

[2] Ifsttar: The French institute of science and technology for transport, development and networks

6. CAPTURING TEXTURE AND SKID RESISTANCE OF THE TESTED SURFACES

To capture the original profiles of the selected surfaces and to measure their skid resistance, the Circular Track Meter (CTM) and the Dynamic Friction Tester (DFT) devices are used respectively (Figure 3) [ASTM E1911; ASTM E1960].

The DFT is equipped with three rubber pads attached to a disc. During the measurement process, driven by a motor, the disc in the "up" position (without contacting the road surface) is accelerated to reach the target speed imposed by the operator. When the required speed is reached, water is sprayed onto the tested surface via a pipe system. The motor then shuts down and the pads are brought into contact with the surface and slide across it. Consequently, the speed of the pads decreases before achieving a total stop due to the friction generated in the pad/road contact patch. The CTM is complementary to the DFT as all texture measurements can be done along the same tracks where DFT measures are done. It measures texture profiles along a circle using a laser mounted upon a rotating arm. The obtained profile is composed of 1024 points scaled at 0.87 mm, meaning a total profile length of 892 mm.

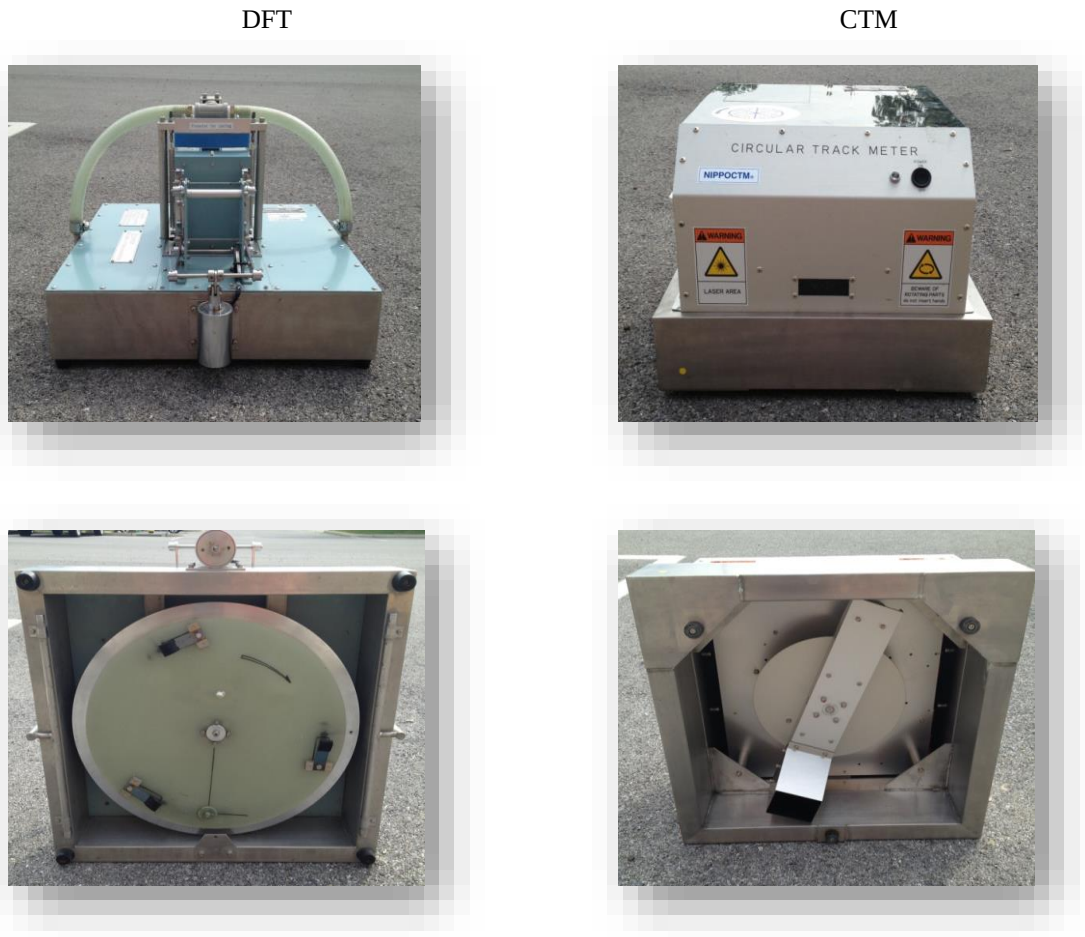

Figure 3: Side (Up) and bottom (Down) views of the DFT (Left) and the CTM (Right)

7. DECOMPOSING THE SURFACE PROFILES AND CREATING THE NEW PROFILES

a. Texture decomposition

The decomposition procedure applied to derive the fundamental IMF of the profiles follows the EMD methodology (Equation 8). The details of that method can be found in Huang's or Kane's publications [Huang et al., 2006; Kane et al., 2014].

$$Z(x) = r_n(x) + \sum_{j=1}^{n} C_j(x) \qquad \text{Equation 7}$$

Where, x represents the distance in the texture profile, Z(x) is the height of a point located at distance x in the profile, $C_j(x)$ is the j^{th} Intrinsic Mode Function (IMF), "n" is the total number of IMF and $r_n(x)$ is the residue obtained after the decomposition.

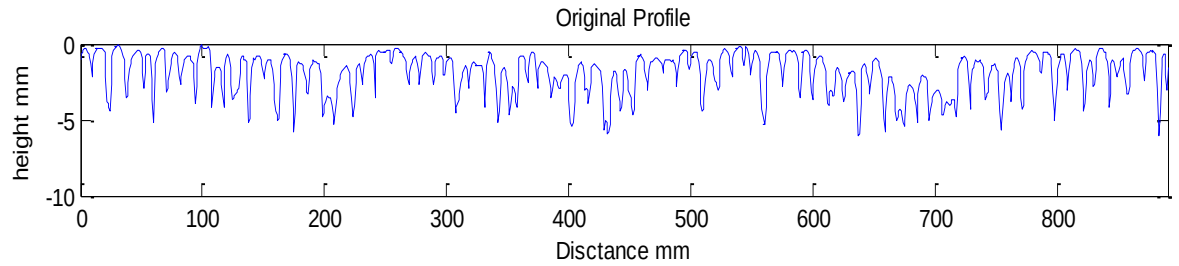

Figure 4: Original profile of the Analytical Surface captured using the CTM

Figure 4 displays the original profile of the Analytical Surface captured using the CTM profilometer. On that profile, the LST (corresponding to the size of the aggregate) and the SST (corresponding to the roughness created by the sandblasting process) are easily distinguishable. Figure 5 displays the IMF of the original profile of the Analytical Surface after applying the EMD procedure:

- IMF 1 captures the smallest intrinsic wavelengths of the original profile. It is assumed to correspond to its SST.
- The IMFs 2 to 5 capture the larger wavelengths of the original profile. It is assumed to correspond to the different scales of the LST of the surface.
- The rest of the IMF, from sixth to ninth, embed larger wavelengths above the LST. These correspond to the undulation and the global slope of the original profile and have no influence on the skid resistance.

Reversely, by summing all the nine profiles, the original profile can be reconstructed.

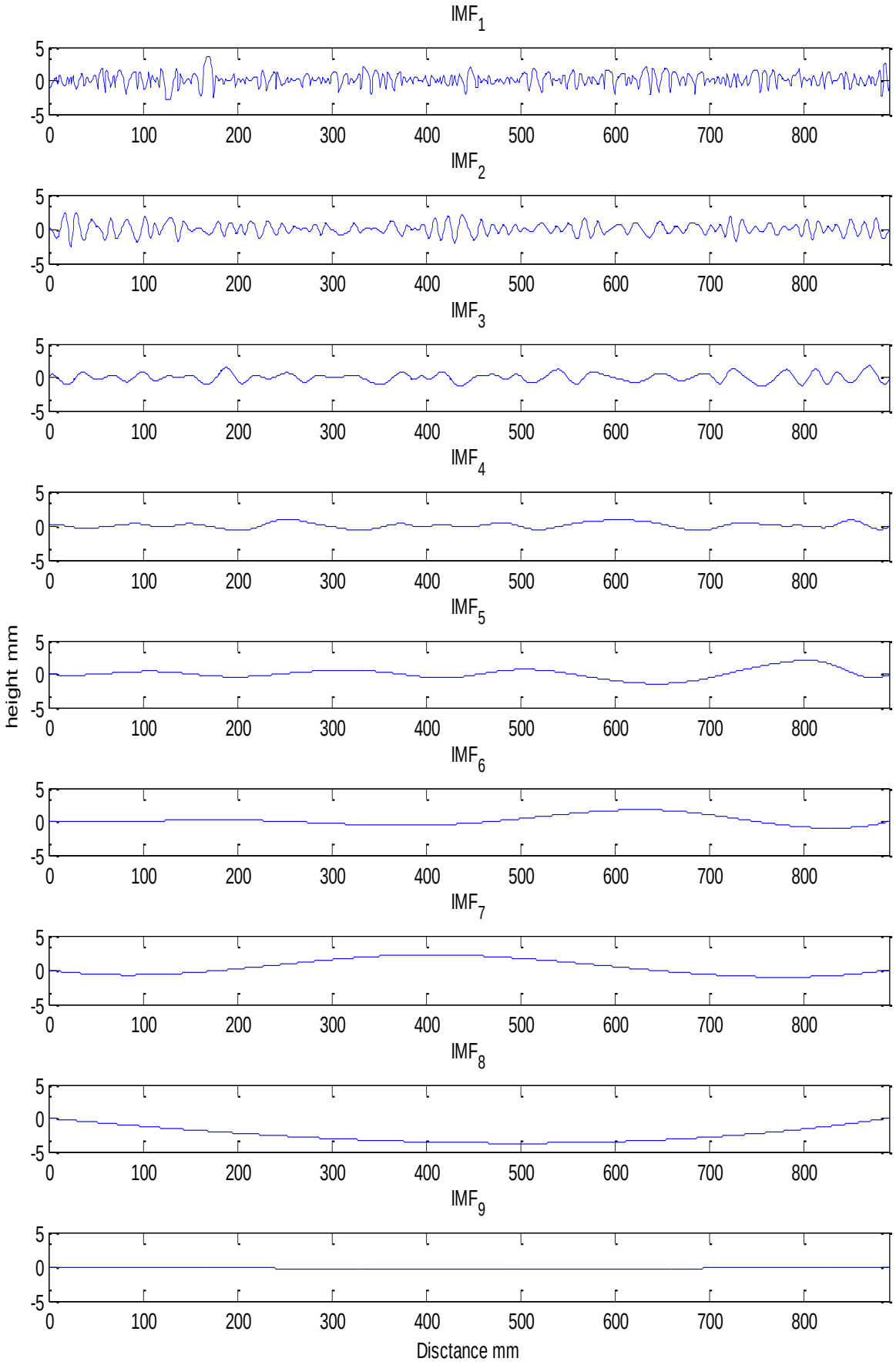

Figure 5: The nine embedded Intrinsic Mode Functions of the Analytical Surface

b. Creation of the new profiles

The new profiles to be analyzed are constructed as follows (see Figure 6):

- The IFMs 1 to 5 are combined to raise a new profile named “Profile 0”. This Profile 0 consists of the SST and LST of the original profile (without the IMFs 6 to 9 that embed the undulation and the slope of the surface).
- IMF 1 is removed from the Profile 0 to derive a profile without SST. This new profile is named “Profile 1”. So, this Profile 1 embeds only LST.
- Then, IMF 2 is removed from the Profile 1 to obtain a second even smoother LST profile compared to Profile 1.

Figure 6 displays the three newly created profiles (Profiles 0 to 2). It can be seen from that figure that Profile 0 is very similar to the original profile.

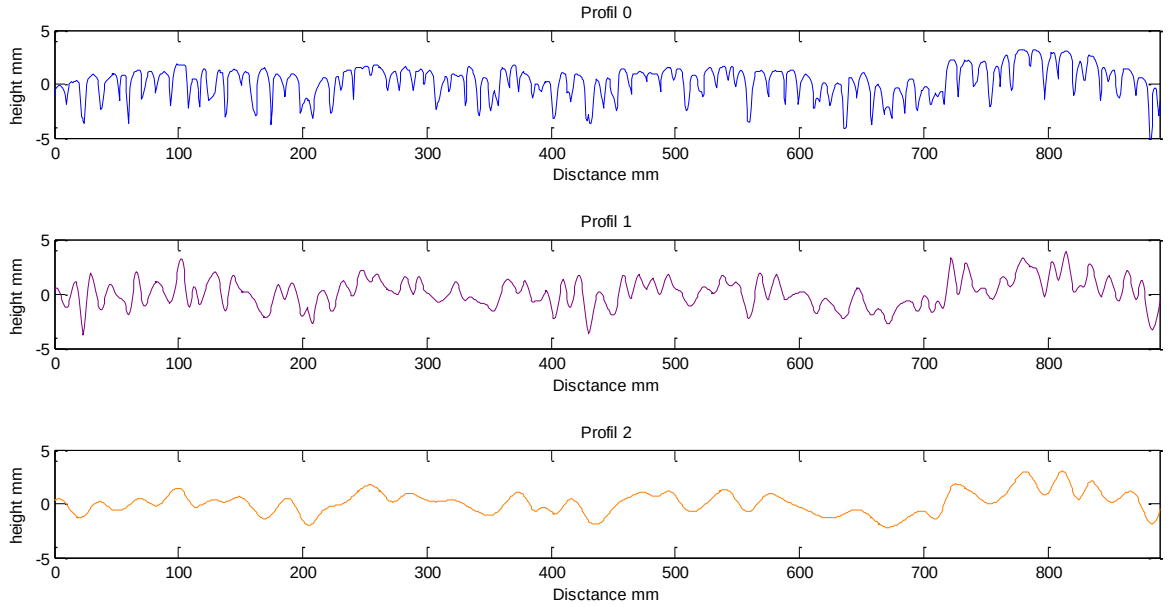

Figure 6: New reconstructed Profiles 0, 1 and 2

8. ANALYSIS PROCEDURE

The overall analysis procedure for each surface is as follows (see figure 7):

- The DFT measures the experimental skid resistance on that real (physical) surface,
- The CTM captures the original profile of that real surface,
- This captured profile gives rise to Profiles 0, 1 and 2 after decomposition and re-composition,
- The DFM (the model) predicts the skid resistance on Profile 0,

- The skid resistance measured by the DFT and the skid resistance predicted by the DFM on Profile 0 (which is roughly the equivalent of the original profile captured with the CTM, but without the undulation and general slope) are compared, this to validate the DFM.
- Once the DFM has been validated, it can be now used to predict the skid resistance that Profiles 1 and 2 would display.

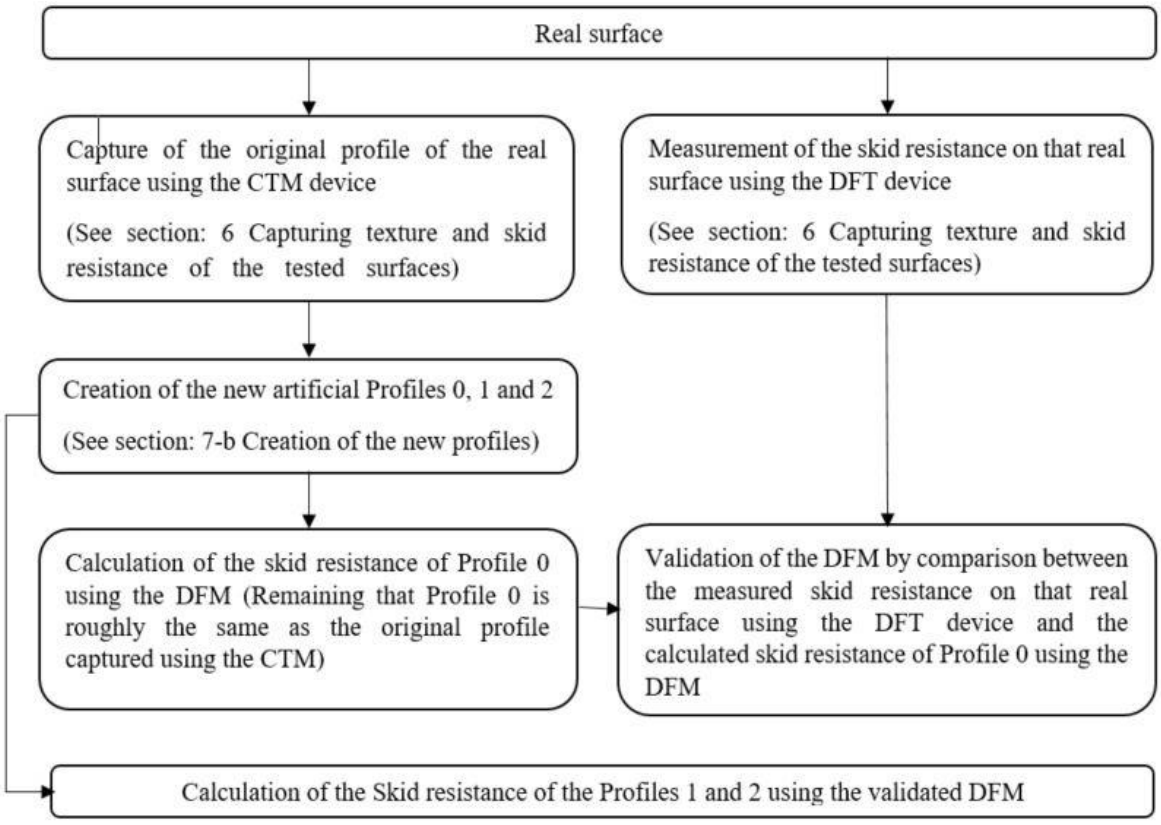

Figure 7: The overall analysis procedure followed for each surface

The DFM is then applied successively to Profiles 0, 1 and 2 at different speeds to calculate their skid resistance. Table 1 displays the inputs used to run the model. These values are related to the DFT (characteristics of the measuring rubber pad, operating conditions) and wetting water [Kane et al., 2017].

For all the surfaces studied, the local friction coefficient μ_{loc} is introduced to take into account the wavelength smaller than 0.87 mm (equation 2). The μ_{loc} is arbitrary set to 0.2 because this value allows the best correspondence of simulations versus experiments skid resistance values of the Analytical Surface. However, maintaining this value equal for all tested surfaces means that the contribution of the wavelengths of the texture lower than the CTM resolution (0.87 mm) is the same for all tested surfaces. This is not necessarily true and may explain the difference between some predicted and experimental results. Indeed, the contribution at these

wavelengths lower than the CTM resolution will depend on microtexture and thereby consequently on the type of aggregate [Tourenq et al., 1971, Forster, 1981, Do et al., 2007].

Table 1: The DFM input parameters

K	**C**	**dx**	**W**	**h**	**l**	**L**	**H_{in}**	**η**
spring's elastic modulus **N/m³**	dashpot's viscosity **N.s/m³**	measuring the resolution of the profiles **mm**	applied load on the rubber **N**	the thickness of the rubber pad **mm**	width of the rubber **mm**	length of the rubber **mm**	Water thickness **mm**	Dynamic viscosity **Pa.s**
$1.4.10^8$	10^2	0.87	11.8	6	16	20	10^{-3}	10^{-3}

9. RESULTS AND DISCUSSION

a. Analytical Surface

Figure 8 displays the estimated skid resistance with the DFM for Profiles 0, 1 and 2 (respectively in blue diamonds, purple triangles, and yellow crosses) of the Analytical Surface at speeds 0 to 100 km/h and the measured skid resistance using the DFT at 20, 40 and 60 km/h (the red squares).

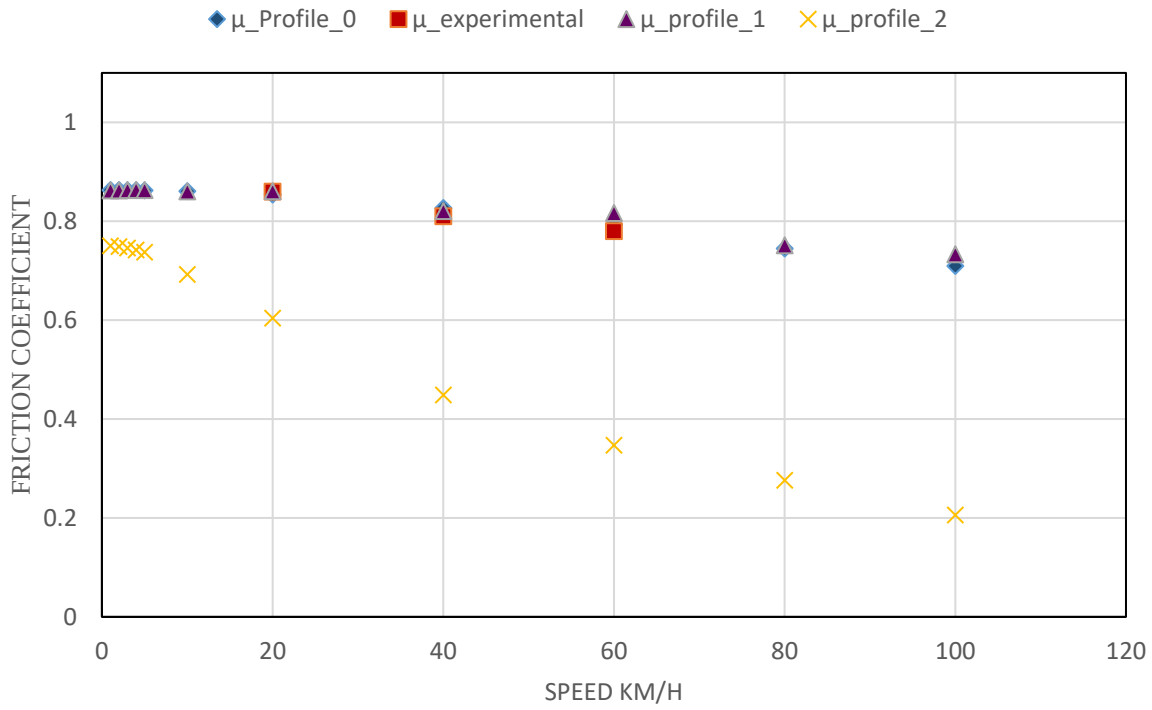

Figure 8: The Analytical Surface – DFM and DFT friction coefficients of Profiles 0, 1 and 2 versus speed

Profiles 0 and 1 derived from the Analytical Surface display the same skid resistance behavior whatever the speed. This similarity is unexpected; as IMF 1 is subtracted from the Profile 0 to create the Profile 1. So normally the latter has less SST and consequently, to be in accordance

with the Horn and Buhlmann's and Sabey's observations [Horn et al., 1983], the skid resistance estimated with the Profile 1 would be shifted down compared to the skid resistance estimated with the Profile 0 at low speeds (but both would maintain roughly the same slope with increasing speed, as both profiles embed roughly the same LST).

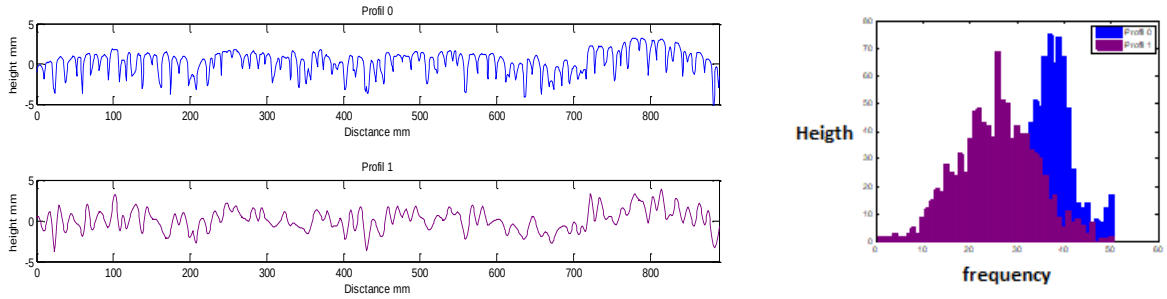

Figure 9: The Profiles 0 and 1 derived from the Analytical Surface on the left and their height distributions on the right

The analysis of the heights distributions of the Profile 0 reveals that the local summits can be almost connected by a flat surface (traduced by a negative skewness of -0.72) whereas, for the Profile 1, it would be connected by a very irregular surface (an almost nil skewness -0.01) (Figure 9). As a result is likely that the rubber pad will encounter more obstacles when it slides over the Profile 1 rather than Profile 0, which tends to generate friction and thus to compensate for the absence of SST. So if the presence of SST has a positive impact on skid resistance, the irregular distribution of the local summits of the LST is also beneficial and can even compensate for a lack of SST.

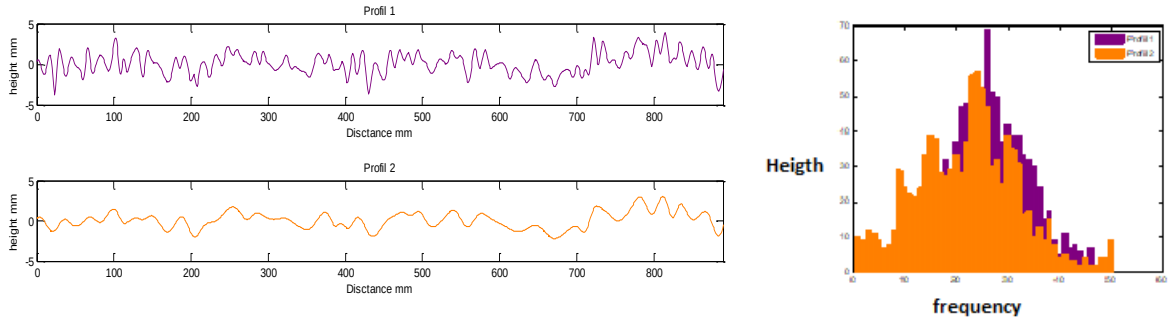

Figure 10: The Profiles 1 and 2 derived from the Analytical Surface on the left and their height distributions on the right

The Profile 2 derived from the Analytical Surface displays lower skid resistance but close to the Profile 1 one at low speed. Indeed, even though both profiles display irregularities of their local summit heights, the Profile 1 embeds more SST than the Profile 2 (Figure 10). With increased speed, the skid resistance drops continuously for Profile 2, this because of its low LST. This behavior is in accordance with some of the works exposed in the introduction section of this paper (Sabey, IFI, Penn State model…) with the SST governing skid resistance at low speeds, and the gradient with increasing speed being governed by the LST.

b. Analysis of the Test-Track Surfaces

To confirm whether the above observations completed on the Analytical Surface, apply to real road surfaces representative of European highway networks, some surfaces selected from the Ifsttar test track are analyzed: a Very Thin Asphalt Concrete 0/6 (VTAC 0/6), a Porous Asphalt 0/6 (PA 0/6), Dense Asphalt Concrete 0./10 (DAC 0/10), a Painted Flexible Asphalt, a Calcined Bauxite Surface Dressing, and a smooth Epoxy Resin (ER).

The asphalt concretes

The three asphalt surfacing (VTAC, PA, and DAC) are similar in terms of texture, embedding the same mean level of both SST and LST. For each of these surfaces, the global shape of their derived three Profiles 0 to 2 display similar LST (contrary to the Profiles 1 and 2 derived from the Analytical Surface) but different SST (See Figures 11 and Figures 14 and 15 of the Appendix).

For these three surfaces, the DFM predicts relatively well the skid resistance measured with the DFT. This is most likely explained by the probable use of the same aggregate type to build these three surfaces, meaning that the contribution of the SST below the CTM resolution is the same and well reflected by the adhesion coefficient set as 0.2 for all the three surfaces within the DFM simulations.

Additionally, for each of the three surfaces, the skid resistance estimated with the DFM of the Profiles 0, 1 and 2 follow the same trend with increasing speeds but are just shifted downward between ones and others. The highest skid resistance at low speed is achieved for Profile 0 (resp. Profile 2) which has the highest (resp. lowest). This behavior is again in accordance with the expectations and agreeing with some of the works exposed in the introduction section of this paper (Sabey, IFI, Penn State model…) which state that the skid resistance at low speed is governed by the SST, and the shape of the curve against speed is related to the LST.

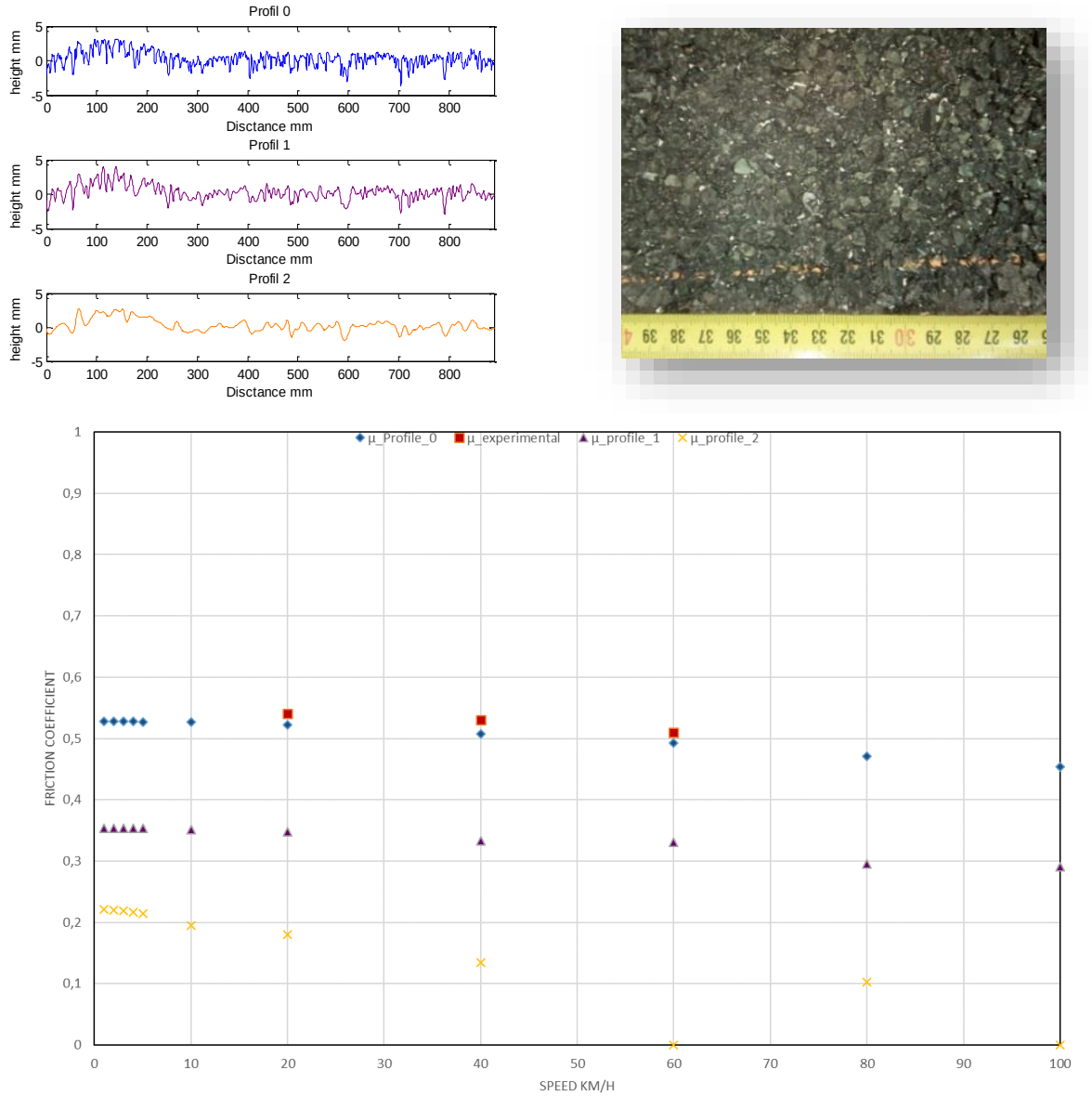

Figure 11: The Very Thin Asphalt Concrete Surface – Up-left: Newly constructed profiles, Up-right: picture of the surface, Bottom: DFM and DFT Skid resistance of Profiles 0, 1 and 2 versus speed

The Painted Flexible Asphalt and the smooth Epoxy Resin

These two surfaces have the particularity of displaying very low SST and LST, possibly even nil for the smooth Epoxy Resin. For the Epoxy Resin, the Profiles 0 to 2 are similar and even all smooth. For the Painted Flexible Asphalt, the Profiles 0 to 2 have similar LST, but differences residing in the presence or not of SST (See Figures 12 and Figure 16 in the Appendix).

For these two surfaces, the DFM predicts relatively low skid resistance (with some instability in the calculations) which is in accordance with the DFT measurements, but not as precise as

for the Asphalt Concrete surfaces. This may again be explained by the use of the same value for the adhesion coefficient, with 0.2 being adopted for all surfaces to proceed to the DFM simulations, a value that may be different in reality for each surface.

Again, for both surfaces, the DFM predictions of the skid resistance for the Profiles 0, 1 and 2 follow the same trend; starting with a low skid resistance at low speed and ending with almost nil value at higher speeds. This behavior is again in accordance with the expectations, low SST means low skid resistance at low speed and low LST leads to the high negative slope of the skid resistance curve against speed.

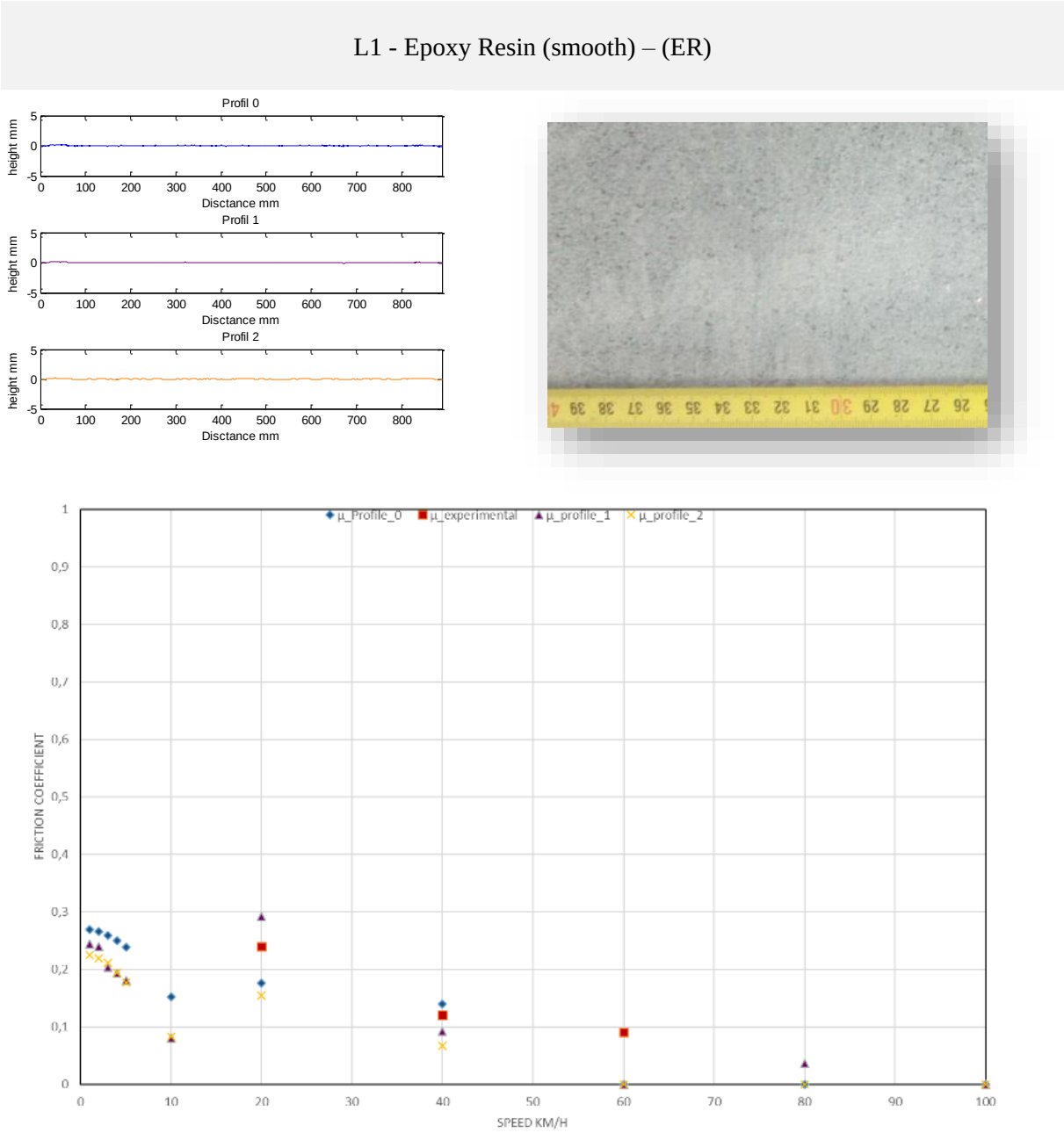

Figure 12: The Epoxy Resin (smooth) Surface – Up-left: Newly constructed profiles, Up-right: picture of the surface, Bottom: DFM and DFT Skid resistance of Profiles 0, 1 and 2 versus speed

The Calcined Bauxite Colgrip

This material is known to provide a high grip surface. The surface is built using sharp calcined bauxite particles of very small size, resulting in good SST, but a mean (or even weak) LST. The three Profiles 0 to 2 derived from this surface are similar in LST: being low but very sharp (conical) shape at their tops of the indentors (Figure 13). For the SST, the ranking is from Profile 0 (very high) to Profile 2 (very low), which was logically expected.

The DFM skid resistance predictions are relatively low in comparison to the DFT measurements. Again, this may be explained by the adhesion coefficient value being set to 0.2 for DFM simulations, whereas this value should be higher for such a micro-rough surface.

The DFM predictions of the skid resistance for the Profiles 0, 1 and 2 follow the same trend with increasing speeds, but Profiles 1 and 2 are shifted significantly downwards compared to Profile 0. The skid resistance of these three profiles does not display a high negative slope despite their low LST. This behavior is unexpected (in accordance with the works exposed in the introduction which state that the skid resistance at low vehicle speed is governed by the SST and the shape of the curve against speed is related to the LST).

The low slope of the skid resistance curve is probably due to the pronounced conicity of the indentors despite the low level of LST. This observation rejoins Forster's who claimed that the most correlated aggregate characteristic to skid resistance is its shape [Forster, 1989]. This means that if the presence of LST is good when the speed increases, the shape of local summits of the SST can be beneficial and can even compensate for the lack of LST.

Even though it should be noted that this random distribution and the pointed shape of the summits may also be an inconvenience with respect to other surface properties such as noise and/or rolling resistance.

F - Calcined Bauxite Colgrip

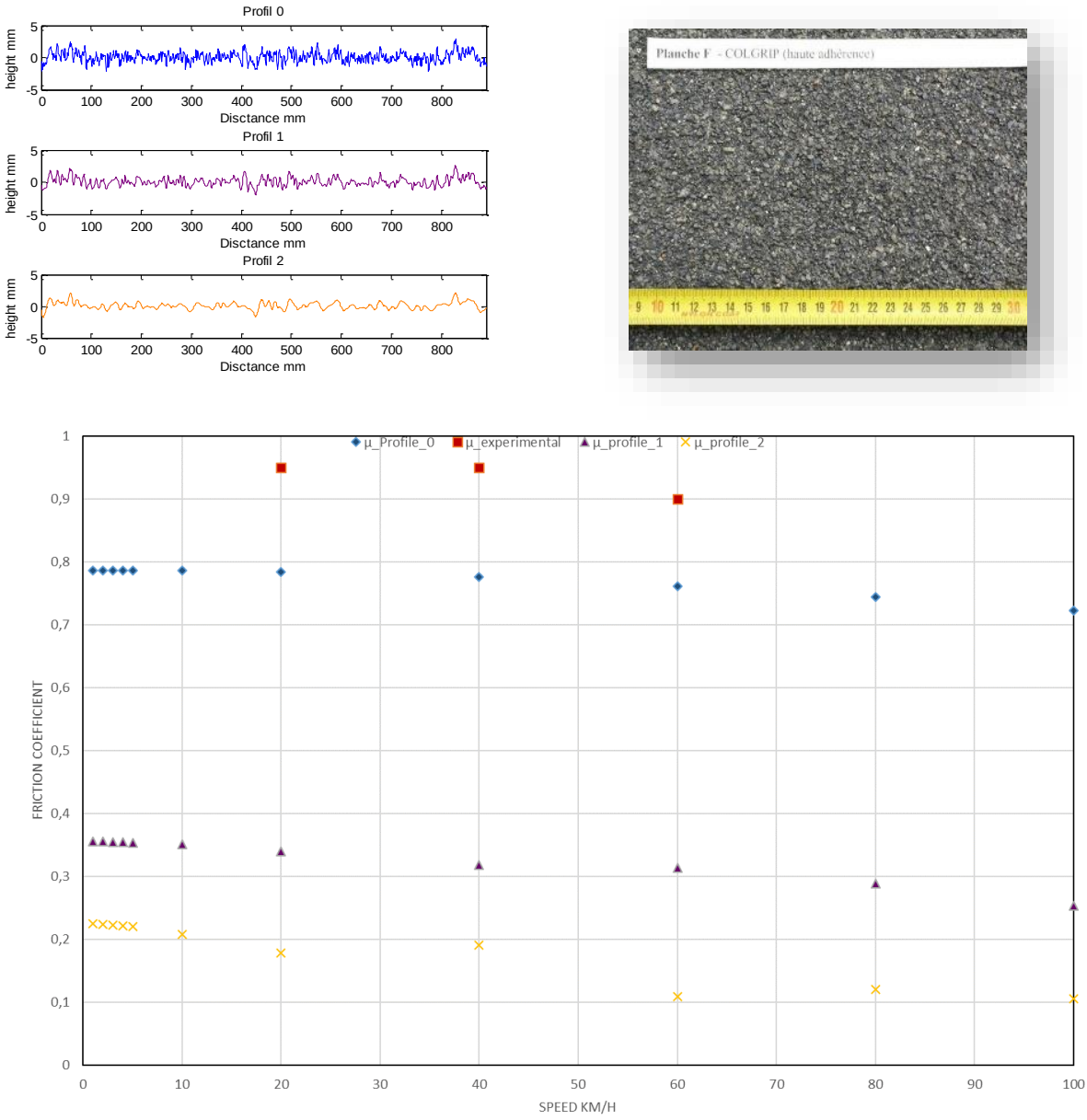

Figure 13: The Calcined Bauxite Colgrip Surface – Up-left: Newly constructed profiles, Up-right: picture of the surface, Bottom: DFM and DFT Skid resistance of Profiles 0, 1 and 2 versus speed

CONCLUSION

This paper aimed to contribute to identifying the role of road surface SST and LST on wet skid resistance. To achieve this, the EMD used to first smoothen at different degrees the textures of selected surfaces and second to apply the DFM on these newly created surfaces to predict their wet skid resistance at different speeds. The results of these simulations showed the importance of both texture scales, but also reveal that the spacial arrangements and shapes of them are just as important. Indeed, on wet road surfaces,

- the SST is key to achieving good skid resistance at low speeds and
- the LST is crucial to maintaining it when the speed increases.
- Also, if the presence of SST is important to improve skid resistance, the distribution of the summits of the LST is also beneficial and can even compensate for the lack of SST.
- And finally, if the presence of LST is important for the maintenance of skid resistance when the speed increases, the shape of local summits of the SST may be also important and can even compensate for the lack of LST.

Even though it should be noted that this random distribution and the pointed shape of the summits may also be an inconvenience with respect to other surface properties such as noise and rolling resistance.

REFERENCES

ASTM E1911, Standard Test Method for Measuring Paved Surface Frictional Properties Using the Dynamic Friction Tester, Developed by Subcommittee: E17.21, Book of Standards Volume: 04.03.

ASTM E1960 - 07(2011), Standard Practice for Calculating International Friction Index of a Pavement Surface, Developed by Subcommittee: E17.21, Book of Standards Volume: 04.03.

ASTM E-1960, 2015. Standard Practice for Calculating International Friction Index of a Pavement Surface. ASTM International, West Conshohocken, PA.ASTM E274/E274M–11, 2011. Standard Test Method for Friction of Paved Surfaces Using a Full-Scale Tire.

ASTM: Calculating International Friction Index of a Pavement Surface, Standard No.E1960-98, ASTM 1998.

Cho C., Stoffels S. M., Rado Z., 2010, Application of Hilbert Huang Transformation to analyze pavement texture-skid resistance relationship, Thesis of the Pennsylvania State University

Do Minh-Tan; Tang Zhenzhong; Kane Malal; Delarrard François, Pavement polishing - Development of a dedicated laboratory test and its correlation with road results, WEAR, Volume: 263, Special Issue: SI Pages: 36-42, 2007

Forster S.W., 1981, Aggregate Microtexture: Profile Measurement and Related Friction Levels, Report FHWA/RD-81/107, Federal Highway Administration, Washington D.C., 36p.

Forster S.W., Pavement Microtexture and Its Relation to Friction, Transportation Research Record, 1989, Vol.1215, pp.151-164.

Fwa T.F., Friction determination for pavement management and wet-weather road safety, International Journal of Transportation Science and Technology, Volume 6, Issue 3, September 2017, Pages 217-227

Gert H., “Hysteresis Friction of Sliding Rubbers on Rough and Fractal Surfaces”, Rubber Chemistry and Technology: March 1997, Vol. 70, No. 1, pp. 1-14

Hall J.W. et al., Guide for Pavement Friction, NCHRP Web-Only Document 108, February 2009, ISBN 978-0-309-42974-0. Available at: https://www.nap.edu/catalog/23038/guide-for-pavement-friction.

Horne, W. and F. Buhlmann., "A Method for Rating the Friction and Micro/Macrotexture Characteristics of Wet Pavements." In STP793-EB Frictional Interaction of Tire and Pavement, edited by WE Meyer and JD Walter, (pp. 191-218). West Conshohocken, PA: ASTM International, 1983. doi:10.1520/STP28524S.

Huang H., Pan J., 2006, Speech pitch determination based on Hilbert-Huang transform, Signal Processing 86 (4), pp. 792–803. DOI:10.1016/j.sigpro.2005.06.011

ISO 13473-2: 2002, Characterization of pavement texture by use of surface profiles - Part 2: Terminology and basic requirements related to pavement texture profile analysis

Kane M., Artamendi I., Scarpas T., Long-term skid resistance of asphalt surfacings: Correlation between Wehner–Schulze Friction values and the mineralogical composition of the aggregates, Wear, Volume 303, Issues 1–2, 15 June 2013, Pages 235-243

Kane M., Cerezo V., 2015. A contribution to tire/road friction modeling: from a simplified dynamic friction contact model to a 'dynamic friction tester' model Wear 342. 163–171. DOI: 10.1016/j.wear.2015.08.007

Kane M., DO M. T., Cerezo V., et al., 2017, Contribution to pavement friction modeling: an introduction of the wetting effect, International Journal of Pavement Engineering, Pages: 1-12, DOI: 10.1080/10298436.2017.1369776

Kane M., Rado Z., and Timmons A., 2014, Exploring the texture–friction relationship: from texture empirical decomposition to pavement friction. International Journal of Pavement Engineering, 16(10), 919–928. doi:10.1080/10298436.2014.9729567

Kane, M., Scharnigg, K. (2009) Report on Different Parameters Influencing Skid Resistance, Rolling Resistance, and Noise Emissions, TYROSAFE project (Tyre and Road Surface Optimisation for Skid Resistance and Further Effects), Deliverable D10

M Kane, V Edmondson, 2018, Modelling the bitumen scour effect: Enhancement of a dynamic friction model to predict the skid resistance of rubber upon asphalt pavement surfaces subjected to wear by traffic, Wear 400, 100-110

Kulakowski B T., Mathematical Model of Friction as a Function of Speed, Transportation Research Board, Issue Number: 1311, p. 26-33, 1991

Leu, M.C., Henry, J.J., 1983. Prediction of Friction as a Function of Speed from Pavement Texture. Transportation Research Record, No. 946, Transportation Research Board, Washington, DC.

Masad, E., et al. (2009) Predicting Asphalt Mixture Friction Based on Aggregate Characteristics. Transportation Research Record Journal of the Transportation Research Board, 2104, 24-33

Rado Z., "Fractal Characterization of Road Surface Textures for Analysis of Friction", International Symposium on Pavement Surface Characteristics, 1996, CHRISTCHURCH, NEW ZEALAND, 1996, p. 101-33, ISBN: 0-86910-711-9

Sabey B.E., 1958, Pressure Distribution beneath Spherical and Conical Shapes Pressed into a Rubber Plane, and their Bearing on Coefficient of Friction under Wet Conditions, Proceedings of the Physical Royal Society, Vol.71, pp 979-988.

Tourenq C., Fourmaintraux D., Propriétés des granulats et glissance routières, Bulletin de Liaison des Laboratoires des Ponts et Chaussées, 51, pp. 61-69, 1971

Villani M., Artamendi I., Kane M., Scarpas A., 2011, The Contribution of the Hysteresis Component of the Tyre Rubber Friction on Stone Surfaces, Journal of the Transportation Research Board, No. 2227, Transportation Research Board of the National Academies, Washington, D.C., pp 153–162

A - Porous Asphalt 0/6 (PA 0/6)

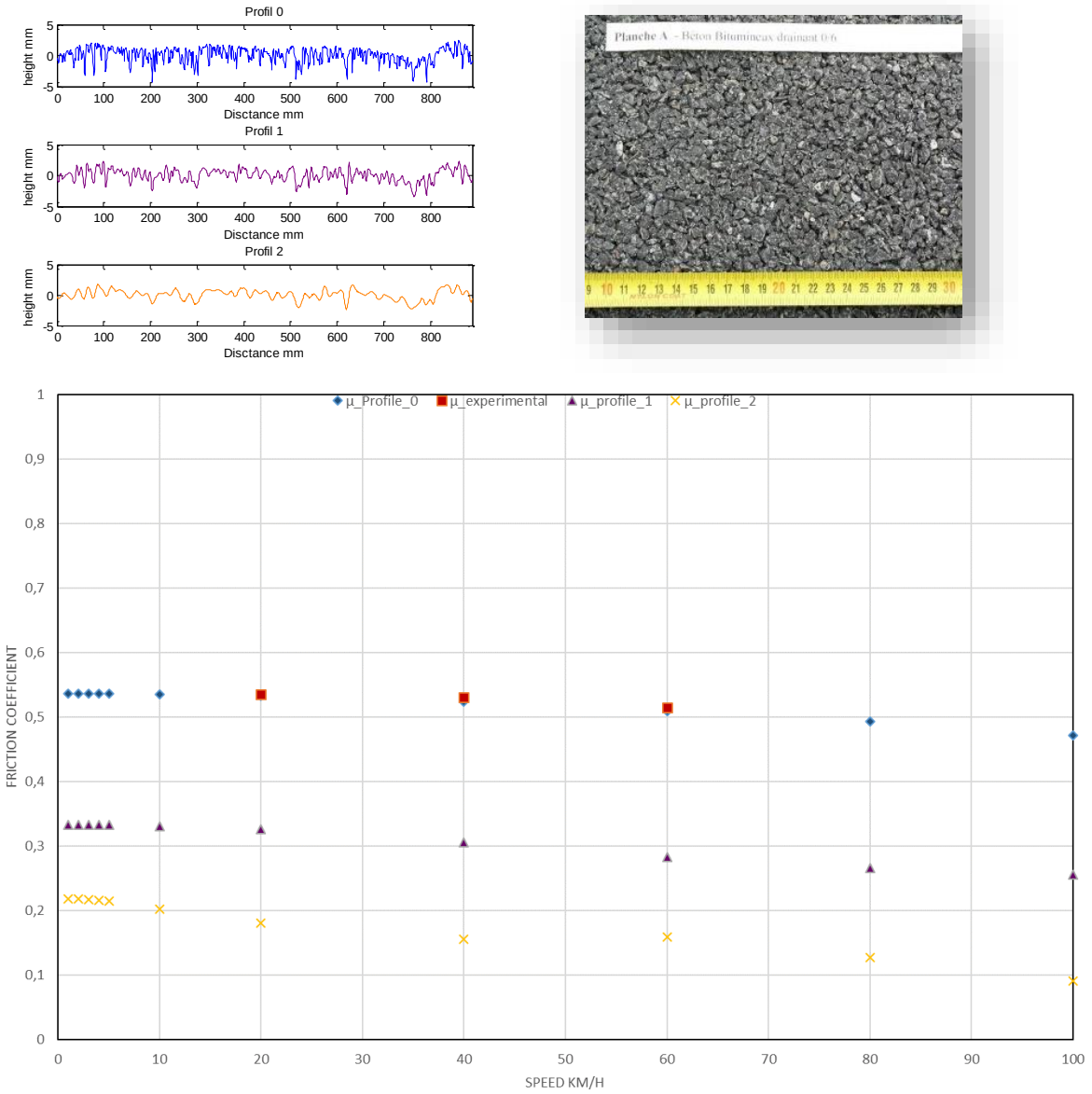

Figure 14: The Very Porous Asphalt Surface – Up-left: Newly constructed profiles, Up-right: picture of the surface, Bottom: DFM and DFT Skid resistance of Profiles 0, 1 and 2 versus speed

E2 - Dense Asphalt Concrete 0./10 (DAC 0/10) – Old

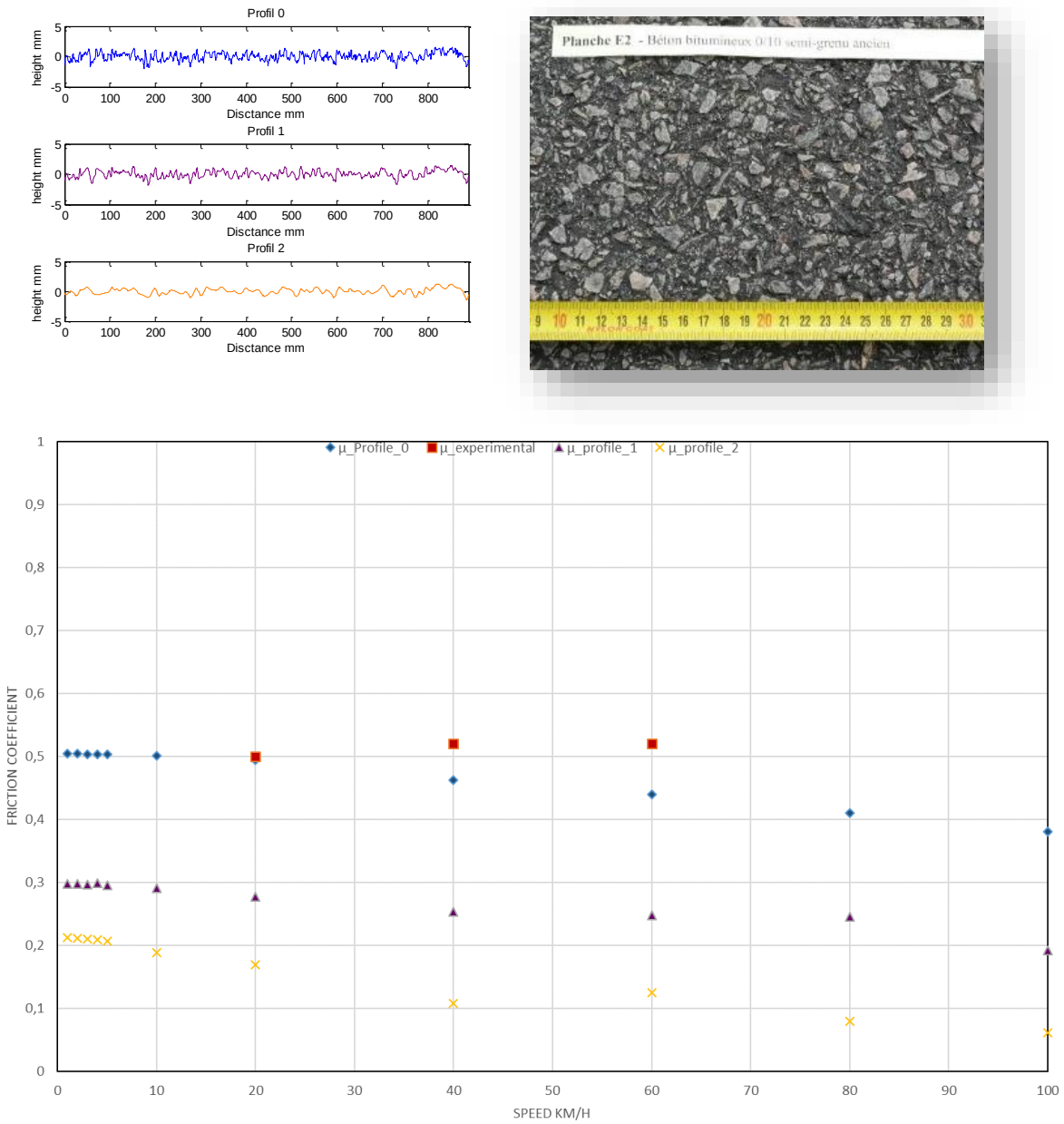

Figure 15: The Dense Asphalt Concrete Surface – Up-left: Newly constructed profiles, Up-right: picture of the surface, Bottom: DFM and DFT Skid resistance of Profiles 0, 1 and 2 versus speed

G1 - Painted Flexible Asphalt

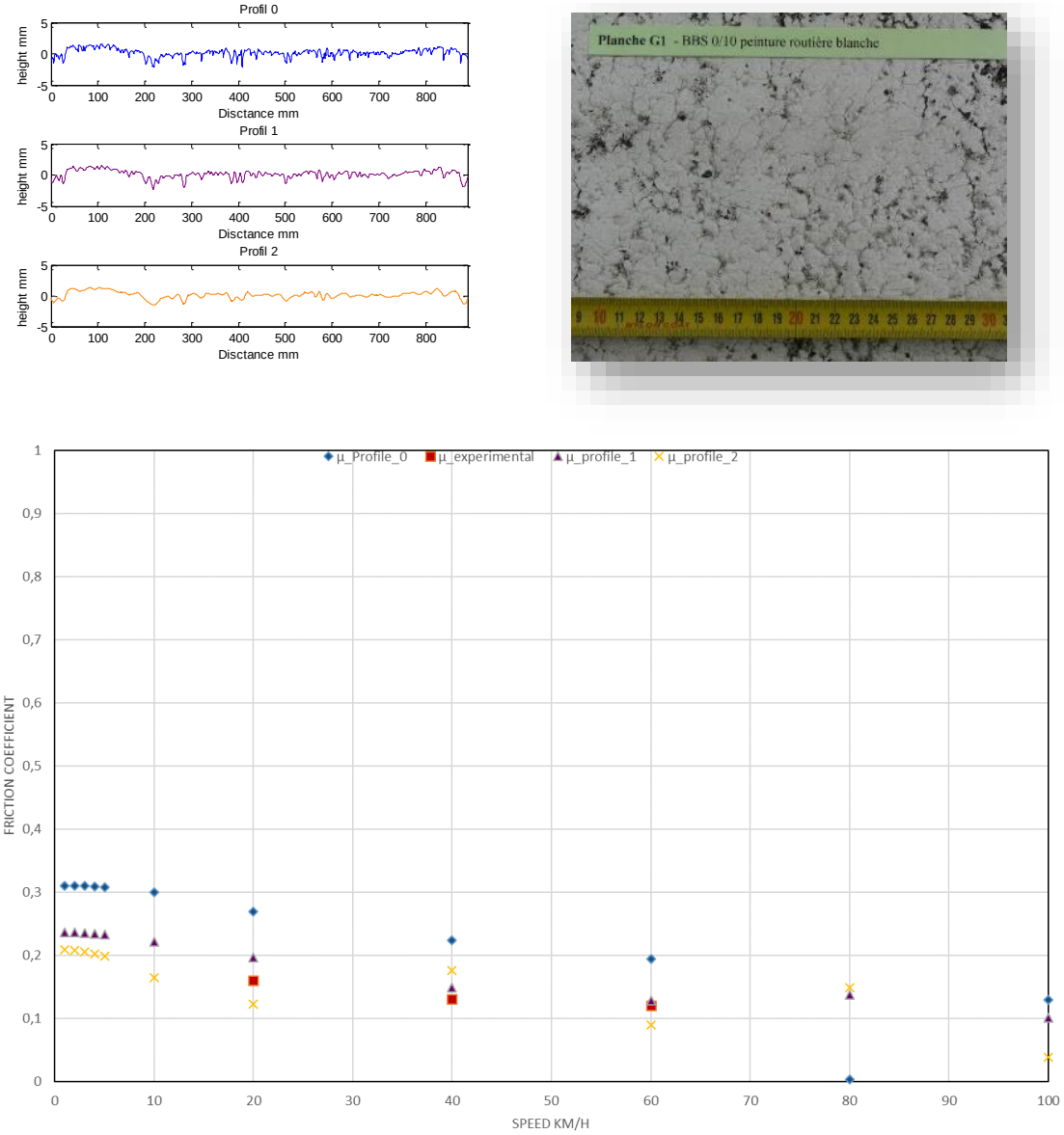

Figure 16: The Painted Flexible Asphalt Surface – Up-left: Newly constructed profiles, Up-right: picture of the surface, Bottom: DFM and DFT Skid resistance of Profiles 0, 1 and 2 versus speed